Drawing and Ultimate Tenacity Properties of Polyamide 6/Attapulgite Composite Fibers

Fang-Chang Tsai,[1] Peng Li,[1] Zhi-Wei Liu,[1] Gang Feng,[1] Ping Zhu,[2] Chuen-Kai Wang,[3] Kan-Nan Chen,[4] Chi-Yuan Huang,[5] Jen-taut Yeh[1,2,3,6,7]

[1]*Ministry of Education, Key Laboratory for the Green Preparation and Application of Functional Materials, Faculty of Materials Science and Engineering, Hubei University, Wuhan, China*
[2]*Key Laboratory of Green Processing and Functional Textiles of New Textile Materials (Wuhan Textile University), Ministry of Education, Wuhan, China*
[3]*Graduate School of Materials Science and Engineering, National Taiwan University of Science and Technology, Taipei, Taiwan*
[4]*Department of Chemistry, Tamgang University, New Taipei City, Taiwan*
[5]*Department of Materials Engineering, Tatung University, Taipei, Taiwan*
[6]*School of Printing and Packaging, Wuhan University, Wuhan, China*
[7]*Department of Polymer Materials, Kun Shan University, Tainan, Taiwan*

Received 27 June 2011; accepted 7 February 2012
DOI 10.1002/app.36970
Published online 18 May 2012 in Wiley Online Library (wileyonlinelibrary.com).

ABSTRACT: The drawing and ultimate tenacity properties of the Polyamide 6 (PA6)/Attapulgite (ATP) composite fiber specimens prepared at varying modified ATP (mATP) contents and drawing condition were systematically investigated. As evidenced by Fourier transform infrared (FTIR) and morphological analysis, demarcated translucent resins were found firmly attached on the surfaces of ATP nanofibers. The specific surface areas of the mATP specimens reached a maximum value at 381 m^2/g as the weight ratios of silane coupling agents to ATP nanofibers reached an optimum value at 1.0. The percentage crystallinity and melt shear viscosity values measured at varying shear rates of $PA6_x(mATP)_y$ specimens increased consistently as their mATP contents increased. In contrast, melting temperatures of $PA6_x(mATP)_y$ specimens reduced slightly as their mATP contents increased. At a fixed drawing temperature and rate, the achievable draw ratio (D_{ra}) values of $PA6_x(mATP)_y$ as-spun fiber specimens approach a maximum value, as their mATP contents are close to the 0.2 wt % optimum value. The maximum D_{ra} values obtained for $PA6_{99.8}(mATP)_{0.2}$ as-spun fiber specimens reached another maximum, when their drawing temperatures and rates approached the optimum values at 120°C and 50 mm/min, respectively. At a fixed draw ratio, the tenacity values of $PA6_x(mATP)_y$ drawn fiber specimens drawn at the optimum drawing temperature and rate reached a maximum value, as their mATP contents approached the 0.2 wt % optimum value. Possible reasons accounting for the interesting morphological, specific surface area, drawing, orientation, and ultimate tenacity properties found for the $PA6_x(mATP)_y$ fiber specimens are proposed. © 2012 Wiley Periodicals, Inc. J Appl Polym Sci 126: 1906–1916, 2012

Key words: attapulgite; fiber; drawing; ultimate tenacity properties

INTRODUCTION

Several attempts have been made to improve the tenacity values of Polyamide 6 (PA6) fibers in the last several decades.[1–6] The achievable draw ratios and ultimate tenacity properties of modified PA6 (MPA) fibers were significantly improved by reactive extrusion PA6 resins with proper amounts of compatibilizer precursors (CP) to prepare MPA resins.[1] At any fixed drawing temperature, the achievable draw ratio (D_{ra}) values of MPA as-spun fiber specimens increase initially with increasing CP contents, and then approach a maximum value, as the CP contents are close to the 5 wt % optimum value. The lengthened PA6 molecules with significantly disrupted hydrogen bonds are expected to draw to higher draw ratios than those PA6 molecules with highly interacted hydrogen bonds but shorter chain lengths, and hence, to result in higher birefringence and achievable draw ratio values after their hot-drawing processes.

On the other hand, the drawing and tensile properties of PA6 fibers were found to improve efficiently after addition of crystallization inhibitors

Correspondence to: J.-t. Yeh (jyeh@mail.ntust.edu.tw).
Contract grant sponsor: Department of Industrial Technology, Ministry of Economic Affairs; contract grant numbers: 95-EC-17-A-11-S1-057, 96-EC-17-A-11-S1-057, 97-EC-17-A-11-S1-057, 99-EC-17-A-11-S1-155, 100-EC-17-A-11-S1-155.
Contract grant sponsor: National Science Council; contract grant numbers: NSC 95-2221-E-253-008-MY3, NSC 99-2221-E-011-010-MY3.

(e.g., carbolic acid[2], naphthalen dicarboxylic acid, isophthalic acid, diphenyl-4,4′ dicarboxylic acid, 4,4′-diphenyl ether dicarboxylic acid,[3] and calcium chloride ($CaCl_2$)[4]). After the addition of $CaCl_2$,[4] the percentage crystallinities and crystallization rates of PA6/($CaCl_2$) fibers increase significantly with the increase in $CaCl_2$ contents. Presumably, the significantly reduced amounts and perfection of crystal phases can help PA6 molecules to unfold and pull out from the crystal lamellas into oriented molecules relatively easy without breaking the taut molecules. In contrast to the crystallization inhibitors, the drawability and ultimate tenacity values of inorganic nanoscale fillers (e.g., carbon nanotubes[5] and clay[6,7]) filled PA6 fibers were found to improve significantly with the inorganic filler contents. The inorganic nanoscale fillers with relatively high specific surface areas can serve as effective nucleation sites to facilitate the crystallization of polymer molecules into relatively poor crystals with low melting temperatures and/or thin lamellar crystals during their crystallization processes. In a way similar to that suggested for crystallization inhibitors-filled PA6 fibers, the crystals with thinner lamellar crystals nucleated by the nanoscale fillers can be melted and/or pulled out of folded lamellar crystals without breaking the taut molecules easier than those from the PA6 crystal phases with lower percentage crystallinity but thicker lamellar crystals in the subsequent hot drawing processes. As a consequence, the drawability and ultimate tenacity values of inorganic fillers-filled PA6 fibers improve significantly as their filler contents increase.

Attapulgite (ATP) is a natural clay mineral together with sepiolite that forms the group of fibrous clay minerals. As shown in Figure 1, its structure scheme was firstly proposed by Bradly in 1940,[8] who described a theoretical formula of $(Mg, Al, Fe)_5Si_8O_{20}(Al)(HO)_2(OH_2)_4{\cdot}4H_2O$. Typical dimensions of ATP are about 0.5–1 μm in length and approximately 10–25 nm across. Many free channels of about 3.8 by 6.3 Å or 5.6 by 11 Å runnig the length of the fibrous structure,[9–12] that can contribute significantly to the specific surface areas of ATP up to an value of about 200 m^2/g.[13] Peng and Chen[14] found that the glass transition temperatures of poly(vinyl alcohol)/ATP nanocomposites increased significantly from 66.1 to 83.7°C, and then reduced to 77.2°C, as their ATP contents increase from 0 to 2 and 7 wt %, respectively. Shen et al.[15] reported that the storage, loss moduli, and dynamic viscosities of PA6/ATP nanocomposites increase with the increase in ATP contents. After melt-blending ATP in PA6 resins, Pan et al.[16] further reported that the yield strengths of PA6/ATP nanocomposites reach a maximun value as their ATP contents approached the optimum content at 4 wt %. As

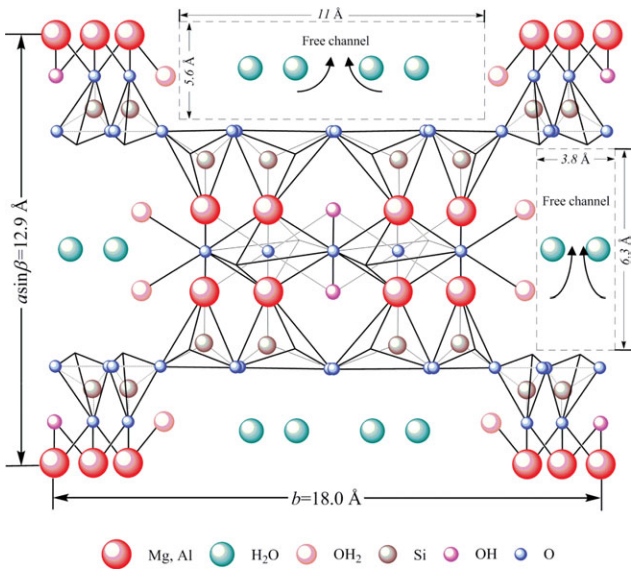

Figure 1 Structure scheme of ATP. [Modified from Ref. 8]. [Color figure can be viewed in the online issue, which is available at wileyonlinelibrary.com.]

suggested by Peng and Chen,[14] the presence of hydroxyl groups on ATP nanofibers with relatively high specific surfaces can provide enormous nucleation sites for attracting polar polymer molecules for nucleation, and hence, facilitate their nucleations during the melt crystallization processes. However, they have never been used as reinforced or functional fibers added in polymeric composites fibers to enhance their ultimate tenacity properties.

In this study, the influence of modified ATP (mATP) contents on the drawing and ultimate tenacity properties of the PA6/mATP composite fiber specimens was investigated. In a way similar to those found for their orientation factor and achievable drawing properties, at a fixed draw ratio, the tenacity values of PA6/mATP drawn fiber specimens drawn at any temperature reach a maximum value, as their mATP contents approach an optimum value. To understand the significantly improved drawing and ultimate tenacity properties, investigations including melt shear viscosity, thermal, and orientation factor analyses were performed on the PA6/mATP resins and/or fiber specimens.

EXPERIMENTAL

Materials and sample preparation

The Zisamide HP1101 PA6 used in this study was obtained from Zig Sheng Industrial Corporation, Taiwan. The ATP powders used in this study were purchased from Jiangsu Prouinge Huaiyuan Mining Coporation, Jiangsu, China. The flow sheet for preparation of mATP nanofibers and PA6/mATP fiber specimens was summarized in Figure 2. The ATP

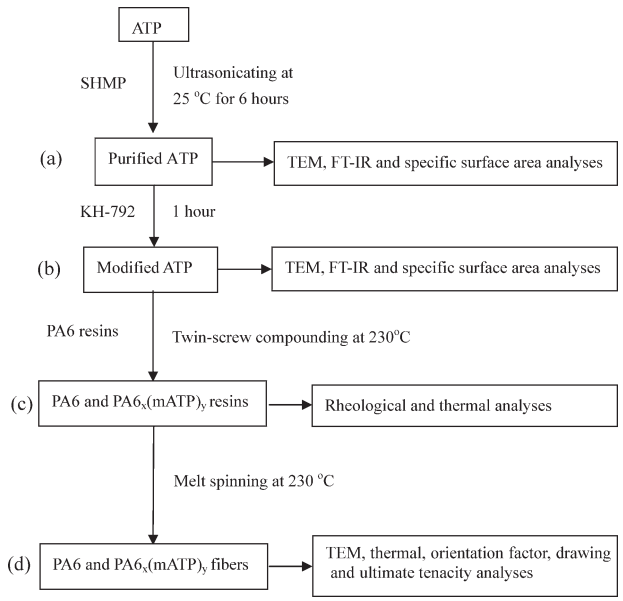

Figure 2 The flow sheet for preparation of mATP nanofibers and $PA6_x(mATP)_y$ fiber specimens.

powders were dispersed and purified using sodium hexametaphosphate (SHMP) in deionized water solutions under ultrasonicating and stirring condition at 25°C for 6 h, wherein 10 g of ATP together with 0.4 g of SHMP were dissolved and dispersed in 0.2 L of deionized water [see Fig. 2(a)]. The opaque purified ATP solutions were then poured out and separated from the sediment impurities. The purified ATP solutions were dried at 80°C for 10 h and then ground into fine powders. A *N*-β-aminoethyl-γ-aminopropyl trimethoxy silane coupling agent with a trade name of KH-792 was used as the surface modifier for purified ATP powders, which was obtained from Diamond Advanced Material of Chemical Corporation, Hubei, China. Before surface modification, deionized water/ethanol solutions (1 : 9 (v/v, mL/mL)) were used to disperse purified ATP powders. The purified ATP powders were ultrasonicated in deionized water/ethanol solutions with a 1 : 20 (w/v, g/mL) composition at 60°C for 3 h to obtain the well dispersed ATP/deionized water/ethanol solutions. About 0.5 mL of KH-792 was then added into 100 mL of ATP/deionized water/ethanol solutions for 1 h [see Fig. 2(b)]. The silane coupling agent mATP powders were then obtained by drying the above prepared ATP/deionized water/ethanol solutions at 80°C in an oven for 10 h. Before further grinding into fine powders, the dried mATP powders were thoroughly washed by ethanol and then dried in a vacuum oven at 40°C for 12 h. The Irganox B1171 antioxidant used in this study was obtained from Ciba-Geigy Corporation, Basel, Switzerland. About 1000 ppm of antioxidant was dry-blended with varying compositions of the dried blends of PA6 resin and mATP powders using a Nanjing Jiant SHJ-20 twin-screw extruder [see Fig. 2(c)]. The extruder was operated at 210°C in the feeding zone and at 230°C toward the extrusion die with a screw speed of 120 rpm. The PA6/mATP blends obtained from twin screw extruder were quenched in cold water at 15°C and cut into the pellet form. The compositions of the PA6/mATP specimens prepared in this study are summarized in Table I.

Prior to spinning, the PA6 and $PA6_x(mATP)_y$ resins were dried in a vacuum oven at 80°C for 16 h. The fiber specimens were then obtained by melt spinning the PA6 and $PA6_x(mATP)_y$ resins using a BCF-FDY single-screw ($L/D = 25$) spinning extruder machine, which was manufactured by San Sheng Chemical Engineering Corporation, Zibo, China [see Fig. 2(d)]. The spinning extruder was operated at 210°C in the feeding zone, 230°C toward the spinneret, and at a screw speed of 100 rpm.

Fourier transform infrared spectroscopy (FTIR)

Fourier transform infrared (FTIR) spectroscopic measurements of the purified ATP and mATP specimens were recorded on a Nicolet Avatar 360 FTIR spectrophotometer at 25°C, wherein 32 scans with a spectral resolution 1 cm^{-1} were collected during each spectroscopic measurement. Infrared spectra of the film specimens were determined by using the conventional KBr disk method. The films used in this study were prepared sufficiently thin enough to obey the Beer–Lambert law.

Specific surface area analysis

A Laser Particle Size Analyzer model BT-9300H (Dandong Bettersize Instruments, Dandong, China) was used to study the specific surface areas of the purified ATP and mATP specimens as discussed in the "Materials and Sample Preparation" section. Ten micrograms of purified ATP and mATP specimens were added and ultrasonicated in 10 mL ethanol at 25°C for 5 min, respectively. The specific surface areas of the purified ATP and mATP specimens were then measured by placing the ultrasonicated

TABLE I
Compositions of PA6 and $PA6_x(mATP)_y$ As-Spun Fiber Specimens

Samples	PA6 (wt %)	Modified ATP (wt %)
PA6	100	0
$PA6_{99.95}(mATP)_{0.05}$	99.95	0.05
$PA6_{99.9}(mATP)_{0.1}$	99.9	0.1
$PA6_{99.8}(mATP)_{0.2}$	99.8	0.2
$PA6_{99.7}(mATP)_{0.3}$	99.7	0.3
$PA6_{99.5}(mATP)_{0.5}$	99.5	0.5

solution specimens prepared above in the cuvette of the Laser Particle Size Analyzer at 25°C.

Morphology analysis

In order to understand the morphologies of the purified ATP, mATP, and their distribution in $PA6_x(mATP)_y$ fibers prepared in "Materials and Sample Preparation" section, the purified ATP and mATP and ultra-cut $PA6_x(mATP)_y$ specimens were dispersed in ethanol and then dried onto a carbon-coated copper grid under ambient conditions prior to examination. A Leica Reichert-Jung Ultracut E Microtome equipped with a diamond knife was used to cut the $PA6_x(mATP)_y$ fibers into 70–90 nm thickness. The specimens prepared above were then observed using a Philip transmission electron microscopy (TEM) model Tecnai G20 operated at 200 kV.

Rheological properties

The melt shear viscosity (η_s) values of the PA6 and $PA6_x(mATP)_y$ resins were measured at 230°C and shear rates ranging from 1000 up to 5000 s^{-1} using a Goettfert Rheotester 1000 Capillary Rheometer equipped with a capillary of 1 mm diameter. Before testing, PA6 and $PA6_x(mATP)_y$ resins were dried in a vacuum oven at 80°C for 16 h. These η_s measured at various shear rates up to about 5000 s^{-1} were used to correlate with the melt-spinning behavior of PA6 and $PA6_x(mATP)_y$ resins, because the shear rates of PA6 melts during melt-spinning were generally recognized to be less than several thousand s^{-1}.

Thermal analysis

The thermal properties of PA6 and $PA6_x(mATP)_y$ resins and/or fibers were determined using a TA differential scanning calorimetry (DSC) model Q100. All scans were carried out at a heating rate of 20 °C/min and under flowing nitrogen at a flow rate of 20 mL/min. Samples weighing 0.5 mg and 15 mg were placed in the standard aluminum sample pans for determination of their melting temperature and percentage crystallinity values, respectively. The percentage crystallinity values of PA6 and $PA6_x(mATP)_y$ specimens were estimated using baselines drawn from 40 to 250°C and a perfect heat of fusion (ΔH_0^f) of PA6 of 230 J/g.[17] The percentages of the crystallinity of the PA6 and $PA6_x(mATP)_y$ resins were calculated as follows.

$$W_c(\%) = \frac{\Delta H_f}{(1-f)\Delta H_f^0} \times 100$$

where ΔH_f is the apparent fusion enthalpy of matrix in the composite and f is the weight fraction of the filler in the composite.

Orientation factors

The orientation factor (f_o) values of the as-spun and drawn PA6 and $PA6_x(mATP)_y$ fiber specimens were measured using a sonic velocity orientation instrument model SCY-III, which was manufactured by Donghuakaili Chemicals and Fiber Technology Corporation, Shanghai, China. Before testing, the fiber specimen with 70 cm in length was wound and clamped on a testing device with a span of 40 cm. The f_o values of the as-spun and drawn fiber specimens were then measured at 25°C. A minimum of five samples of each specimen were tested and averaged during the orientation measurements.

Drawing and ultimate tenacity properties

The fiber specimens used in the drawing experiments were cut from the as-spun fibers and then stretched on a Gotech tensile testing machine Model GT-TFS-2000 equipped with a temperature-controlled oven. The dimensions of the cut fibers are 100 mm in length, which were wound and clamped in a stretching device and drawn at varying temperatures to investigate the temperature dependence of the drawability of the fiber specimens at a fixed drawing rate of 50 mm/min. The temperatures used in the drawing process were 60, 80, 100, 110, 120, 130, and 140°C. The draw ratio of each specimen was determined as the ratio of the marked displacement after and before drawing. The marked displacement before drawing was 30 mm. The tensile properties of the as-spun and drawn fibers were determined using the Gotech tensile testing machine Model GT-TFS-2000 at 25°C and a crosshead speed of 50 mm/min. Five samples of each specimen were tested and averaged during the tensile experiments.

RESULTS AND DISCUSSION

Fourier transform infrared spectroscopy

FT-IR spectra of purified ATP and mATP specimens are shown in Figure 3. Distinguished absorption bands centered at 479/507 (doublet), 985/1028 (doublet), 1195, 1654, 3404 3553, 3582, and 3615 cm^{-1} were found in the spectrum of the purified ATP specimen, which are generally attributed to the motions of Si—O—Si bending vibration,[18] Si—O stretching vibration,[19] Si—O—Si stretching vibration,[20–22] O—H bending,[20,23] and stretching[18] vibration in coordinated and zeolite water, Si—OH stretching vibration,[24] Al—Fe—OH stretching vibration,[24] and Al—Al—OH stretching vibration[20,24] of purified ATP specimens, respectively. The above distinguished absorption bands appearing in the spectrum of the purified ATP specimen were also found in the FTIR spectrum of the mATP specimen. However, distinguished absorption

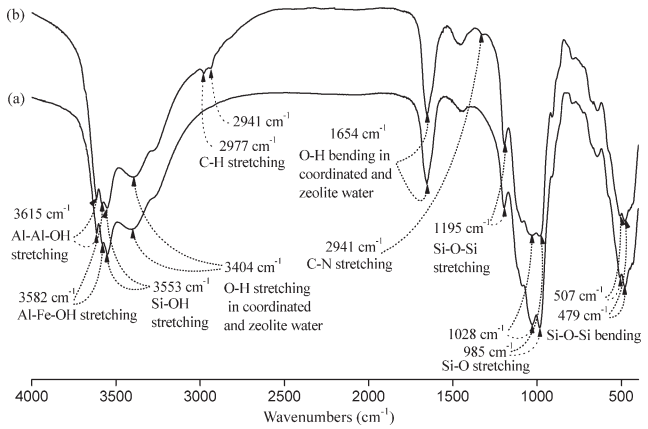

Figure 3 FTIR spectra of (a) purified ATP and (b) mATP specimens.

bands corresponding to the motions of Si—O stretching vibration bands observed in the spectrum of mATP specimen are significantly larger than those of the purified ATP specimen. In contrast, the absorption band corresponding to the motion of Si—OH stretching vibration centered at 3553 cm^{-1} in the spectrum of the mATP specimen is significantly smaller than that of the purified ATP specimen. The new absorption bands centered at 1322, 2941/2977 (doublet) cm^{-1} found in the spectrum of mATP specimen are attributed to the stretching vibration motion of C—N and C—H groups originally present in the silane coupling agent, respectively. The enhancement of Si—O stretching vibration bands and reduction of Si—OH stretching vibration bands are attributed to the reaction of CH_3—OH and Si—OH groups of the hydrolyzed silane coupling agent and Si—OH groups of purified ATP specimen during the surface modification process of mATP specimen.

Morphology analysis

Typical TEM micrographs of purified ATP and mATP specimens dispersed in ethanol are shown in Figure 4(a–d). As shown in Figure 4(a,b), typical fibrous structure was observed for the purified ATP specimen, in which the length and thickness of the ATP nanofiber are around 500 and 20 nm, respectively. After surface modification, dimensions of mATP nanofibers remained relatively unchanged. However, some translucent resins were found attaching firmly on the surface of the mATP specimens [see Fig. 4(c,d)]. As evidenced by FTIR analysis in the previous section, the attached translucent resins found on the surfaces of mATP specimens suggested that the silane coupling agent was successfully grafted to ATP nanofibers through the reaction of CH_3—OH or Si—OH groups of the hydrolyzed silane coupling agent and Si—OH groups present on the surfaces of purified ATP nanofibers.

Typical TEM micrographs of $PA6_x(mATP)_y$ fiber specimens were summarized in Figure 5. As shown in Figure 5(a,b), mATP nanofibers were found relatively well dispersed in $PA6_x(mATP)_y$ fiber specimens with mATP contents lower than 0.5 wt %. In contrast, somewhat aggregated mATP nanofibers were found on the micrograph of $PA6_{99.5}(mATP)_{0.5}$ fiber specimen [see Fig. 5(c)].

Specific surface area analysis

The specific surface areas of the purified ATP and mATP specimens are summarized in Figure 6. A high specific surface area at 360 m^2/g was found for the purified ATP specimen. After surface modification by a silane coupling agent, the specific surface areas of the mATP specimens increased initially with the increase in the weight ratios of silane coupling agents to ATP nanofibers and reached the maximum value at 381 m^2/g as the weight ratios of silane coupling agents to mATP nanofibers reached an optimum value at 1.0. The specific surface areas of the mATP specimens then reduced reversely from 381 to 320 m^2/g as the weight ratios of silane coupling agents to ATP nanofibers increase from 1.0 to 2.0, respectively. As evidenced by morphology and FTIR analysis in the previous sections, the significant increased specific surface areas of mATP specimens is attributed to the grafted silane coupling agent, which did not overwrap but attached firmly on the surfaces of mATP specimens.

Rheological properties

Figure 7 exhibits the melt shear viscosity (η_s) values of PA6 and $PA6_x(mATP)_y$ resins measured at 230°C and at varying shear rates. The η_s values of PA6 and $PA6_x(mATP)_y$ resins reduce significantly as the shear rates increase. In contrast, the η_s values of $PA6_x(mATP)_y$ resins measured at varying shear rates increase significantly as their mATP contents increase. For instance, at a fixed shear rate of 2000 1/s, the η_s values of $PA6_x(mATP)_y$ resins measured at 230°C increase significantly from 226.7 to 233.8, 242.4, 253.9, 259.5, and 270.1 Pa s, as their mATP contents increase from 0 to 0.05, 0.1, 0.2, 0.3, 0.5 wt %, respectively. Apparently, at mATP contents equal to or less than 0.5 wt %, the mATP nanofibers were well dispersed in PA6 melt during the preparation and melt-blending processes of $PA6_x(mATP)_y$ resins. In which, the mATP nanofibers are likely to entangle and hinder the melt flow of PA6 molecules during the measurements of their η_s values at varying shear rates, and hence, results in significant increase in η_s values of $PA6_x(mATP)_y$ resins as their mATP contents increase.

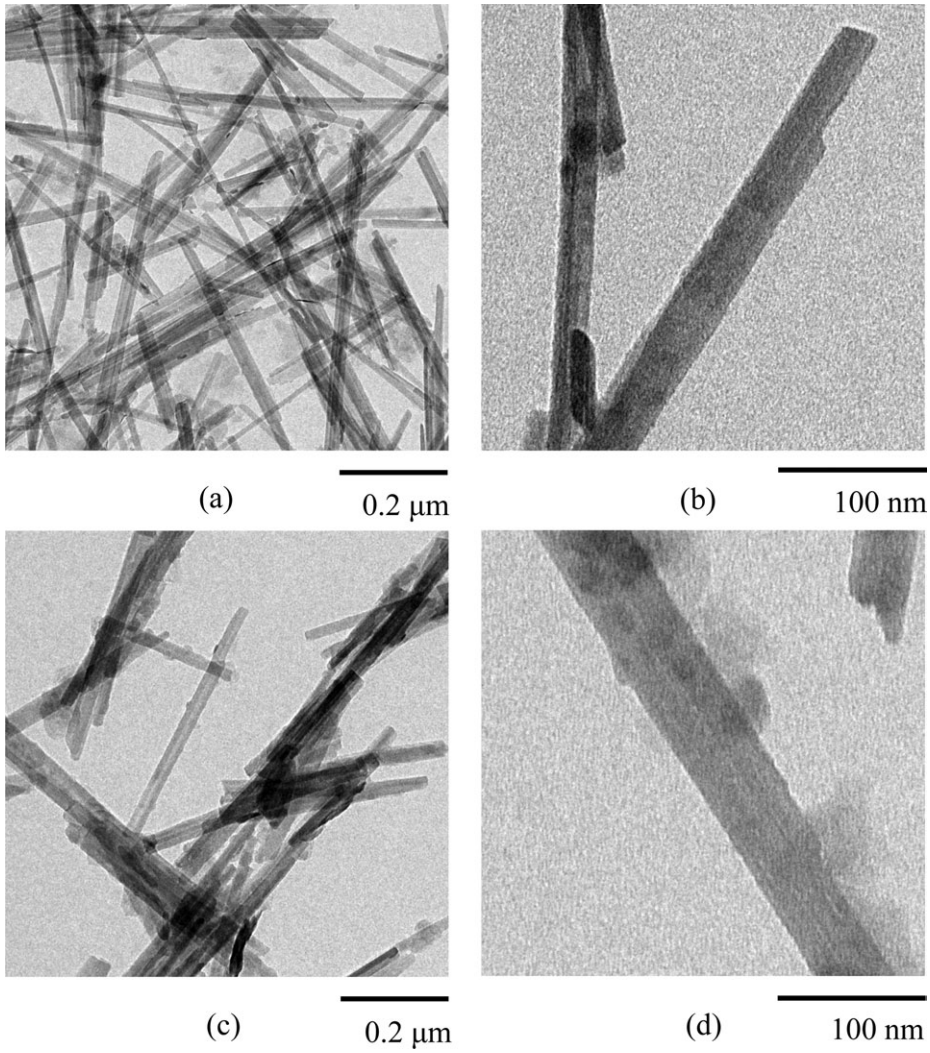

Figure 4 TEM micrographs of purified ATP specimens photographed at magnification of (a) 86,000, (b) 236,000 and mATP specimens at a magnification of (c) 86,000 and (d) 236,000.

Thermal analysis

Typical differential scanning calorimetry (DSC) heating and cooling thermograms of PA6 and $PA6_x(mATP)_y$ as-spun fiber specimens are shown in Figures 8 and 9, respectively. As shown in Figure 8, a main melting endotherm with a peak temperature at 220.6°C was found on the DSC thermogram of the PA6 as-spun fiber specimen. After blending 0.05, 0.1, 0.2, 0.3, and 0.5 wt % mATP nanofibers in PA6 resins, the melting temperature (T_m) values of $PA6_x(mATP)_y$ fiber specimens reduced slightly from 220.4 to 220.3, 220.2, 220.1, and 219.9°C, respectively. In contrast, their percentage crystallinity (W_c) values increased significantly from 28.7 to 29.1, 30.3, 31.6, and 32.5%, respectively, as the mATP contents increase from 0 to 0.05, 0.1, 0.2, 0.3, and 0.5 wt %. The values of onset ($T_{c\text{-onset}}$) and peak ($T_{c\text{-peak}}$) temperatures shown on the crystallization exotherms of $PA6_x(mATP)_y$ as-spun fiber specimens increased significantly from 187.6/183.6°C to 188.7/185.8°C, 188.9/186.0°C, 189.0/186.1°C, 189.5/186.8°C, and to 189.8/187.3°C, respectively, as their mATP contents increase from 0 to 0.05, 0.1, 0.2, 0.3, and 0.5 wt %. These results suggest that mATP nanofibers with relatively high specific surface areas can serve as effective nucleation sites to facilitate the crystallization of PA6 molecules into relatively poor and/or thin lamellar crystals with low melting temperatures during their melt crystallization processes.

Achievable drawing properties

Figure 10 summarizes the values of achievable draw ratio (D_{ra}) of PA6 and $PA6_x(mATP)_y$ as-spun fiber specimens drawn at varying temperatures but at a fixed drawing rate of 50 mm/min. At a fixed drawing temperature and rate, the D_{ra} values of $PA6_x$ $(mATP)_y$ as-spun fiber specimens increase initially with the increase in the mATP contents, and then approach a

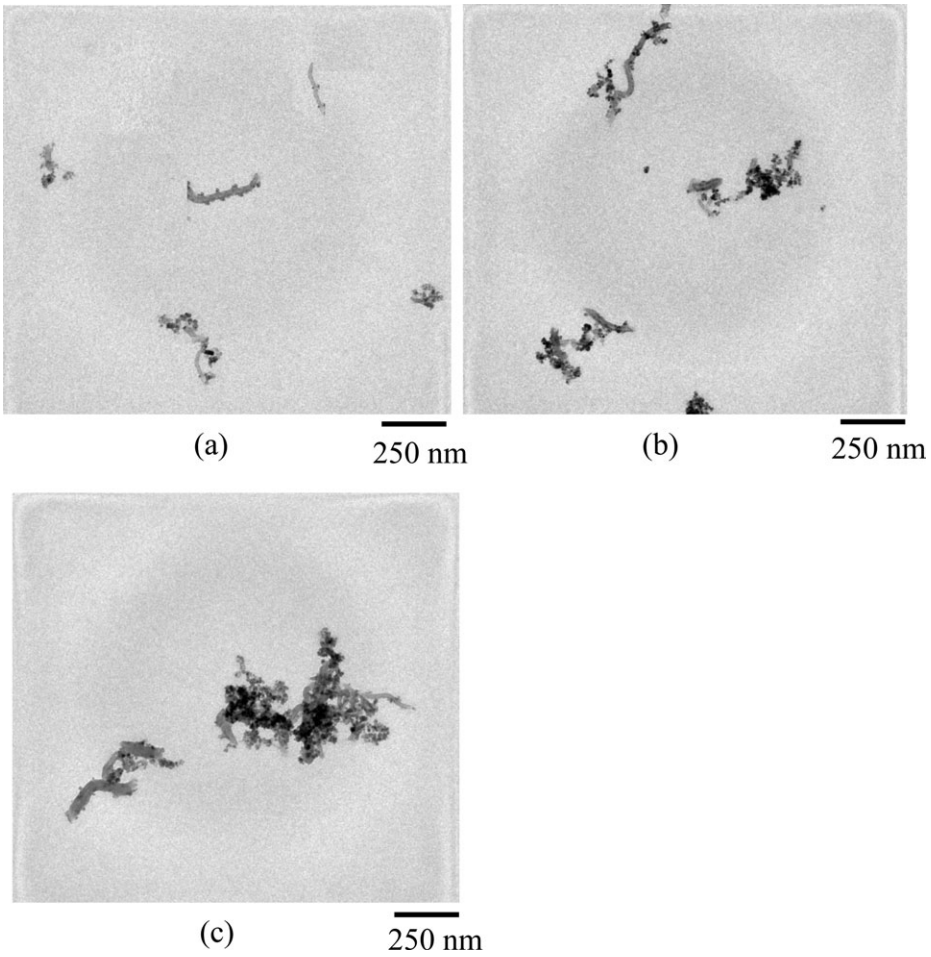

Figure 5 TEM micrographs of (a) $PA6_{99.9}(mATP)_{0.1}$, (b) $PA6_{99.8}(mATP)_{0.2}$, and (c) $PA6_{99.5}(mATP)_{0.5}$ fiber specimens photographed at a magnification of 8600.

maximum value, as the mATP contents are close to the 0.2 wt % optimum value. For instance, at a drawing temperature of 80°C, the D_{ra} values of the $PA6_x(mATP)_y$ as-spun fiber specimens increase from 5.7 to 6.9 and to 5.8, as their mATP contents increase from 0 to 0.2 and 0.5 wt %, respectively. The maximum D_{ra} values obtained for $PA6_{99.8}(mATP)_{0.2}$ as-spun fiber specimens prepared at the 0.2 wt % optimum mATP content further increase with the drawing temperatures and reach another maximum as their drawing

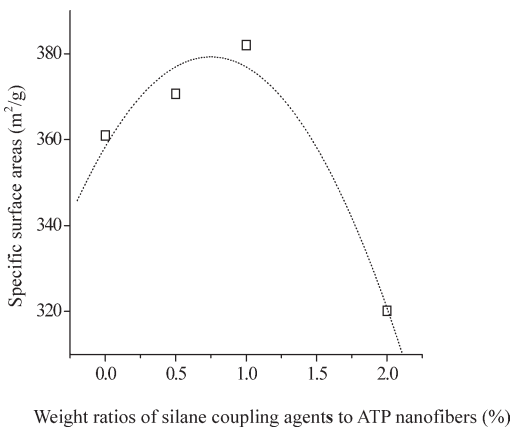

Figure 6 Specific surface areas of mATP (□) specimens prepared at varying weight ratios of silane coupling agents to ATP nanofibers.

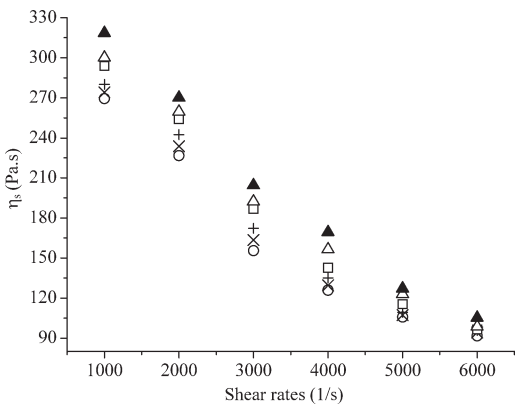

Figure 7 Melt shear viscosity (η_s) values of PA6 (○), $PA6_{99.95}$ $(mATP)_{0.05}$ (×), $PA6_{99.9}$ $(mATP)_{0.1}$ (+), $PA6_{99.8}$ $(mATP)_{0.2}$ (□), $PA6_{99.7}$ $(mATP)_{0.3}$ (△), and $PA6_{99.5}$ $(mATP)_{0.5}$ (▲) specimens.

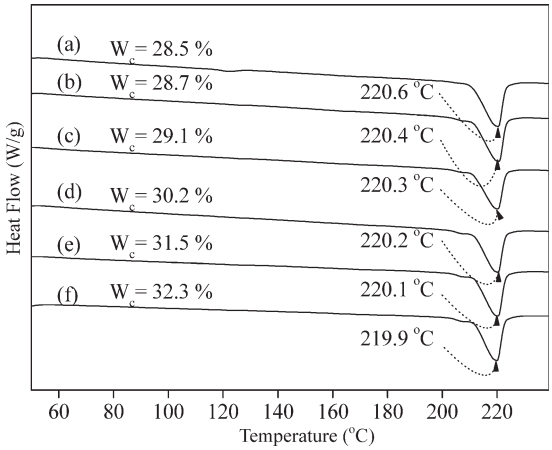

Figure 8 DSC heating thermograms of (a) PA6, (b) $PA6_{99.95}(mATP)_{0.05}$, (c) $PA6_{99.9}(mATP)_{0.1}$, (d) $PA6_{99.8}(mATP)_{0.2}$, (e) $PA6_{99.7}(mATP)_{0.3}$, and (f) $PA6_{99.5}(mATP)_{0.5}$ specimens scanned at 20 °C/min.

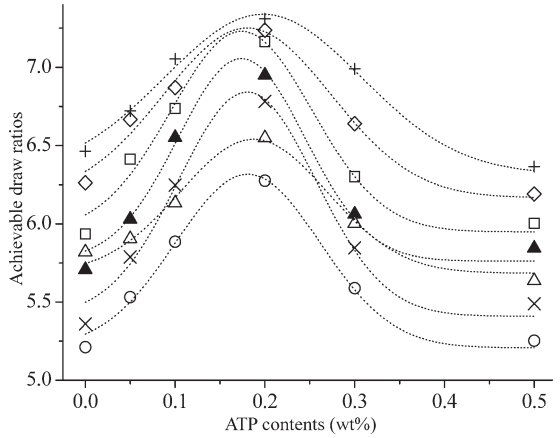

Figure 10 Achievable draw ratios of $PA6_x(mATP)_y$ as-spun fiber specimens drawn at 25 (○), 60 (×), 80 (▲), 100 (□), 110 (◇), 120 (+), and 140°C (△) and a drawing rate of 50 mm/min.

temperatures approach the optimum drawing temperature at 120°C. At drawing temperatures higher than 120°C, their D_{ra} values reduce with the increase in drawing temperatures. For instance, the D_{ra} values of $PA6_{99.8}(mATP)_{0.2}$ as-spun fiber specimens increase from 6.7 to 7.3 and then reduce reversely to 6.5, as their drawing temperatures increase from 60 to 120 and 140°C, respectively.

Figure 11 summarizes the values of achievable draw ratio (D_{ra}) of $PA6_{99.8}(mATP)_{0.2}$ as-spun fiber specimens drawn at 120°C and varying drawing rates. It is worth noting that D_{ra} values of $PA6_{99.8}(mATP)_{0.2}$ as-spun fiber specimens prepared at the optimum mATP content and drawing temperature increase initially with the increase in the drawing rates and then approach a maximum value, as the drawing rates are close to the optimum drawing rate of 50 mm/min. For instance, D_{ra} values of $PA6_{99.8}(mATP)_{0.2}$ as-spun fiber specimens increase from 6.1 to 7.30 and 6.1, as their drawing rates increase from 10 to 50 and 90 mm/min, respectively.

Orientation factors

The orientation factor (f_o) values of PA and $PA6_x(mATP)_y$ fiber specimens prepared at varying drawing temperatures and draw ratios are summarized in Figure 12. As expected, f_o values of PA6 and $PA6_x(mATP)_y$ fiber specimens increased significantly with the increase in their D_{ra} values. It is worth noting that, at a fixed draw ratio, the f_o values of $PA6_x(mATP)_y$ drawn fiber specimens drawn at any temperature reach a maximum value, as their mATP contents approached the 0.2 wt % optimum value. For instance, at a D_{ra} of 5, the f_o values of $PA6_x(mATP)_y$ fiber specimens drawn at 60°C increased

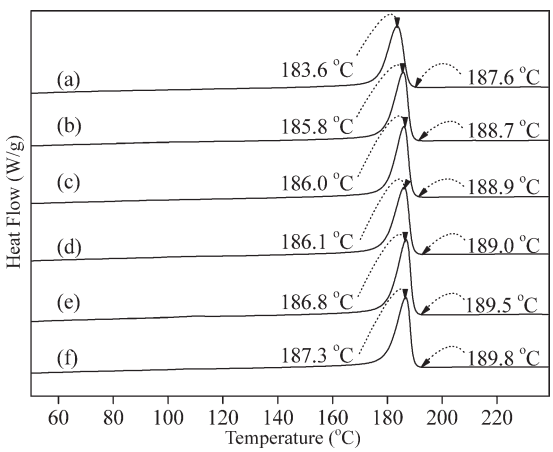

Figure 9 DSC cooling thermograms of (a) PA6, (b) $PA6_{99.95}(mATP)_{0.05}$, (c) $PA6_{99.9}(mATP)_{0.1}$, (d) $PA6_{99.8}(mATP)_{0.2}$, (e) $PA6_{99.7}(mATP)_{0.3}$, and (f) $PA6_{99.5}(mATP)_{0.5}$ specimens scanned at 20 °C/min.

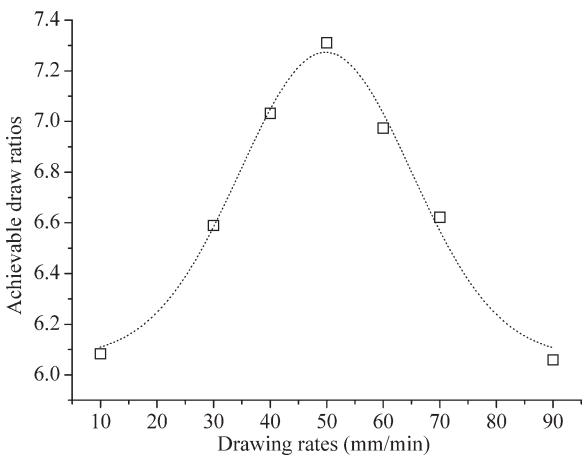

Figure 11 Achievable draw ratios of $PA6_{99.8}(mATP)_{0.2}$ as-spun fiber specimens drawn at 120°C and varying drawing rates.

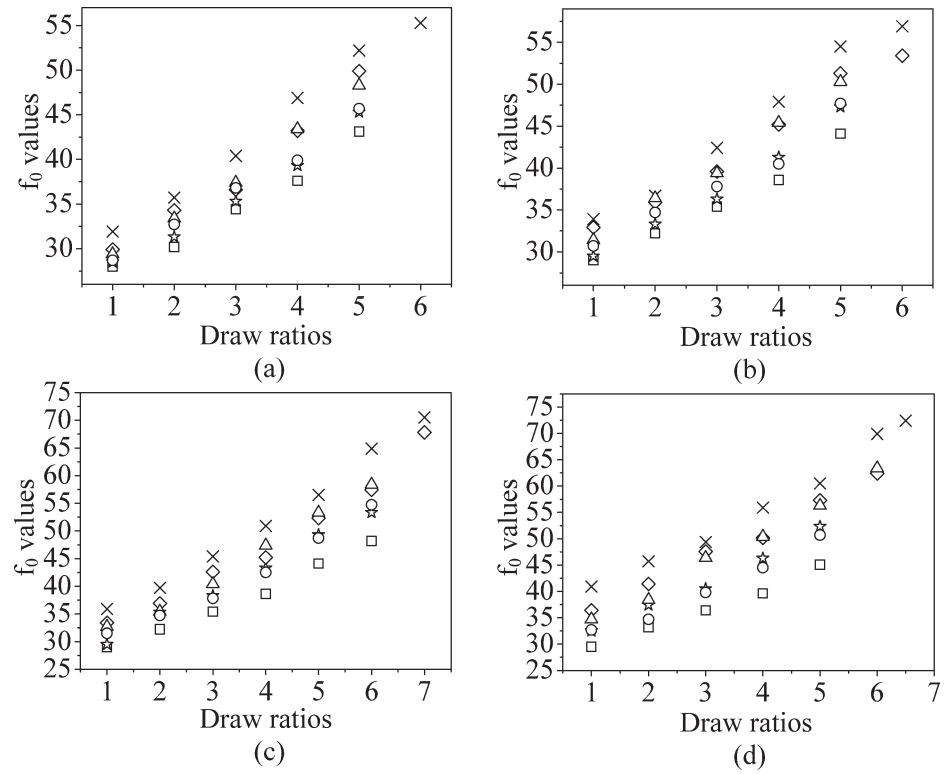

Figure 12 The f_o values of PA6(□), $PA6_{99.95}(mATP)_{0.05}$(☆), $PA6_{99.9}(mATP)_{0.1}$(◇), $PA6_{99.8}(mATP)_{0.2}$(×), $PA6_{99.7}(mATP)_{0.3}$(△), and $PA6_{99.5}(mATP)_{0.5}$(○) fiber specimens drawn at 50 mm/min and (a) 25, (b) 60, (c) 120, and (d) 140°C.

from 44.1 to 54.5 and then reduced to 47.7, as their mATP contents increased from 0 to 0.2 and 0.5 wt %, respectively. As expected, the maximum f_o value obtained for $PA6_{99.8}(mATP)_{0.2}$ drawn fiber specimens with a fixed draw ratio further increased significantly as their drawing temperatures increased from 25 to 140°C.

As evidenced by thermal analysis, the melting temperature and/or crystal perfection present in $PA6_x(mATP)_y$ as-spun fiber specimens reduce with increasing mATP contents, although the amounts of less perfect crystals with lower melting temperatures and/or smaller crystal thickness increase significantly as their mATP contents increase. Presumably, these less perfect crystals with lower melting temperatures and/or smaller crystal thickness obtained at higher mATP contents can be melted and pulled out of folded lamellar crystals relatively easily during drawing processes, and hence, results in higher drawability and orientation of the $PA6_x(mATP)_y$ fibers. However, the amounts of coagulated mATPs are likely to increase significantly when their ATPs contents are higher than certain values. These coagulated mATP nanofibers can slide with each other and serve as the defects during the drawing processes of $PA6_x(mATP)_y$ as-spun fiber specimens, and hence lead to a significant reduction in their achievable draw ratios and orientation factor values. Based on these premises, it is reasonable to understand that the achievable draw ratios of $PA6_x(mATP)_y$ as-spun fiber specimens and/or orientation factor values of the $PA6_x(mATP)_y$ fibers with a fixed draw ratio reduce significantly when their mATP contents are higher than the specific optimum values.

Tenacity properties

Figure 13 summarizes the tenacity values of the as-spun and drawn PA6 or $PA6_x(mATP)_y$ fiber specimens drawn at 120°C the optimum drawing temperature and 50 mm/min the optimum drawing rate. As expected, the tenacity values of PA6 and $PA6_x(mATP)_y$ as-spun fiber specimens improved consistently as their draw ratios increased. In a way similar to those found for their orientation factor properties, at a fixed draw ratio, the tenacity values of $PA6_x(mATP)_y$ drawn fiber specimens reached a maximum value, as their mATP contents approached the 0.2 wt % optimum value, and then reduced reversely with the further increase in mATP contents. For instance, at a D_{ra} value of 5, the tenacity values of $PA6_x(mATP)_y$ drawn fiber specimens increased from 4.45 g/day to 4.71 g/day and then reduce to 4.05 g/day, when their mATP contents increased from 0 to 0.2 and 0.5 wt %, respectively. In fact, at 0.2 wt % optimum mATP content, the

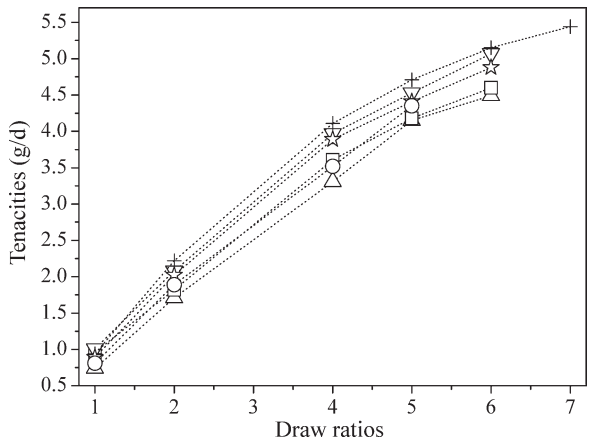

Figure 13 Tenacity values of PA6 (△), $PA6_{99.95}$ $(mATP)_{0.05}$ (□), $PA6_{99.9}$ $(mATP)_{0.1}$ (▽), $PA6_{99.8}$ $(mATP)_{0.2}$ (+), $PA6_{99.7}$ $(mATP)_{0.3}$ (☆), and $PA6_{99.5}$ $(mATP)_{0.5}$ (○) drawn fibers drawn at 120°C and 50 mm/min.

tenacity values of $PA6_{99.8}(mATP)_{0.2}$ fiber specimens drawn at the optimum drawing temperature and rate can reach near 5.5 g/day, which is about 25% higher than that of the PA6 fiber drawn at 120°C and 50 mm/min.

The mechanical properties of the drawn specimens are generally believed to depend mainly on the degree of orientation of the drawn specimens, as their molecular weights are constant.[25,26] As evidenced by the orientation factor analysis, at a fixed draw ratio, the orientation factor values of drawn $PA6_{99.8}(mATP)_{0.2}$ fiber specimens prepared at the optimum mATP content are always higher than those of $PA6_x(mATP)_y$ fiber specimens prepared at other mATP contents, respectively. These results clearly suggest that a good orientation of PA6 molecules along the drawing direction can have a beneficial effect on the tensile properties of the $PA6_x$ $(mATP)_y$ fibers. Excellent orientation and tensile properties of the $PA6_x(mATP)_y$ fibers can be obtained by preparing them at the optimum mATP contents, in which, even better drawing, orientation and tenacity properties can be obtained for $PA6_x$ $(mATP)_y$ fiber specimens by using proper drawing temperatures and rates.

CONCLUSIONS

Demarcated translucent resins were found firmly attaching on the surfaces of mATP specimens. As evidenced by FTIR analysis, the attached translucent resins were the successfully grafted silane resins, which were formed through the reaction of CH_3—OH or Si—OH groups of the hydrolyzed silane coupling agent and Si—OH groups present on the surfaces of purified ATP nanofibers. The specific surface areas of the mATP specimens increased initially with the increase in the weight ratios of silane coupling agents to ATP nanofibers and reached the maximum value at 381 m^2/g as the weight ratios of silane coupling agents to ATP nanofibers reached an optimum value at 1.0. The W_c, $T_{c\text{-onset}}$, $T_{c\text{-peak}}$ values, and η_s measured at varying shear rates of $PA6_x$ $(mATP)_y$ specimens increased consistently as their mATP contents increased. In contrast, T_m values of $PA6_x(mATP)_y$ specimens reduced slightly as their mATP contents increased.

At any fixed drawing temperature, the D_{ra} values of $PA6_x(mATP)_y$ as-spun fiber specimens increased initially with the increase in mATP contents, and then reached a maximum value, as their mATP contents approached the 0.2 wt % optimum value. The maximum D_{ra} values obtained for $PA6_{99.8}(mATP)_{0.2}$ as-spun fiber specimens reached another maximum, when their drawing temperatures and rates approached the optimum values at 120°C and 50 mm/min, respectively. At a fixed draw ratio, the f_o and ultimate tenacity values of $PA6_x(mATP)_y$ drawn fiber specimens drawn at the optimum temperature and rate reached a maximum value, as their mATP contents approached the 0.2 wt % optimum value. These results clearly suggest that a good orientation of PA6 molecules along the drawing direction has a beneficial influence on the tensile properties of the $PA6_x(mATP)_y$ fibers, which can be obtained by preparing the fibers at an optimum mATP content and drawing condition.

References

1. Wei, W.; Wang, X. L.; Liu, Z. W.; Wu, D. R.; Qiu, L.; Tsai, F. C.; Lai, Y. C.; Zhu, P.; Yeh, J. T. Polym Eng Sci 2011, 51, 755.
2. Takeyama, S.; Kuroda, N.; Suga, K. (Yokohama Rubber Co Ltd) Jpn Pat.10,016,137 (1998).
3. Robert, M.; Arno, E. (HNA Holdings Inc. [US]) U.S. Pat. 6,426, 128 (2002).
4. Wei, W.; Qiu, L.; Wang, X. L.; Chen, H. P.; Lai, Y. C.; Tsai, F. C.; Zhu, P.; Yeh, J. T. J Polym Res 2011, 18, 1841.
5. Bessell, T.; Shortall, J. B. J Mater Sci 1975, 10, 2035.
6. Xie, S. B.; Zhang, S. M.; Liu, H. J. Polymer 2005, 46, 5417.
7. Yeh, J. T.; Wang, C. K.; Liu, Z. W.; Li, P.; Tsou, C. H.; Lai, Y. C.; Tsai, F. C. Polym Eng Sci, 2012.
8. Bradley, W. F. Am Miner 1940, 24, 405.
9. Frost, R. L.; Cash, G. A.; Kloprogge, J. T. Vib Spectrosc 1998, 16, 173.
10. Christ, C. L.; Hathaway, J. C.; Hostetler, P. B.; Shepard, A. O. Am Miner 1969, 54, 198.
11. Drits, V. A.; Sokolova, G. V. Soviet Phys Crystallogr 1971, 161, 183.
12. Mark, P. S.; Stephen, G. Appl Clay Sci 2008, 39, 98.
13. Haden, W. L. Attapulgite: properties and uses. In: Tenth National Conference on Clays and Clay Minerals, held at Austin, Texas, 1961; Vol. 3, p 284.
14. Peng, Z. Q.; Chen, D. J. J Polym Sci Part B: Polym Phys 2006, 44, 534.
15. Shen, L.; Lin, Y. J.; Du, Q. G.; Zhang, W.; Yang, Y. L. Polymer 2005, 46, 5758.
16. Pan, B. L.; Yue, Q. F.; Ren, J. F.,Wang, H. G.; Jian, L. Q.; Zhang, J. Y.; Yang, S. R. Polym Test 2006, 25, 384.

17. Wunderlich, B. Crystal Melting. Macromolecular Phys; Academic Press: New York, 1980; Vol. 3.
18. Augsburger, M. S.; Strasser, E.; Perino Mercader, R. C.; Pedregosa, J. C. J Phys Chem Solids 1998, 59, 175.
19. Blanco, C.; González, F.; Pesquera, C.; Benito, I.; Mendioroz, S.; Pajares, J. A. Spect Lett 1989, 22, 659.
20. Mendelovici, E. Clay Clay Miner 1973, 21, 115.
21. Yariv, S. Clay Miner 1986, 21, 925.
22. Vicente-Rodríguez, M. A.; Suarez, M.; Bañares-Muñoz, M. A.; Lopez-Gonzalez, J. de. D. Spectochim Acta A 1996, 52, 1685.
23. Mendelovici, E.; Portillo, D. C. Clay Clay Miner 1976, 24, 177.
24. Chali, A.; Petit, S.; Decarreau, A. Clay Clay Miner 2002, 50, 306.
25. Paul, S.; Piet, J. L. Polymer 1980, 21, 1341.
26. Brigitte, V.; Alain, P.; Claude, C.; Cédric, S.; René, P.; Catherine, J.; Patrick, B.; Philippe, P. Science 2000, 290, 1331.